DOI: https://doi.org/10.37434/tpwj2024.12.01

COATING FOR MEDICAL APPLICATION PRODUCED BY MICROPLASMA SPRAYING FROM Zr–Nb ALLOY

S.Yu. Maksymov[1], S.G. Voinarovych[1], S.N. Kaliuzhnyi[1], O.N. Kyslytsia[1], I.S. Sviridova[1], L. Alontseva[2], Ridvan Yamanoglu[3]

[1]E.O. Paton Electric Welding Institute of the NASU
11 Kazymyr Malevych Str., 03150, Kyiv, Ukraine
[2]D. Serikbayev East Kazakhstan Technical University
19 Serikbayev Str., 070004, Ust-Kamenogorsk, Kazakhstan
[3]Department of Metallurgical and Materials Engineering,
Faculty of Engineering, Kocaeli University, Kocaeli 41001, Turkey

ABSTRACT

The work deals with the technology of microplasma spraying of biocompatible coatings from Zr–Nb alloy and their properties. On the surface of a porous Zr–Nb coating with the most developed surface microrelief, the presence of both open macropores of up to 300 μm in size and micropores of up to 10 μm in size was revealed. The X-ray phase analysis of the formed Zr–Nb coatings showed the presence of phases of α-solid solution of Zr, oxide (ZrO_2), nitride (ZrN) and carbide ($ZrNbC_2$). The corrosion resistance of a microplasma Zr–Nb coating and Ti6Al4V alloy in a solution of 0.9 % NaCl, which simulates the environment of the human body, was determined. It is assumed that Zr–Nb alloy coatings produced by microplasma spraying on the surfaces of existing Ti6Al4V alloy endoprostheses will allow for the future improvement in corrosion resistance and osseointegration between the bone and the implant.

KEYWORDS: microplasma spraying, biocompatible coating, Zr–Nb alloy, surface morphology, adhesion strength, corrosion resistance

INTRODUCTION

Currently, the titanium-based alloy of the Ti6A14V alloying system is the most widely used in the manufacture of orthopaedic implants [1]. However, the bioinertness of the surface of Ti6A14V alloy implants negatively affects the formation of a functional bonding between the implant and the bone [2]. In addition, long-term operation of Ti6A14V alloy implants in close contact with human bone and soft surrounding tissues leads to the release of alloying elements such as vanadium and aluminium and the manifestation of pathological reactions in the body. For example, aluminium interferes with bone mineralization, leading to structural deficiencies, while vanadium is highly cytotoxic and can cause allergic reactions [3].

Since the implant surface is the first to interact with the surrounding living tissue after implantation, the characteristics of the implant surface (such as its topography, hydrophilicity, roughness, etc.) play a dominant role both in the interaction of cells with the metal implant as well as in the subsequent processes of its osseointegration [4].

It is possible to increase the biocompatibility of existing Ti6A14V alloy implants by modifying their surface to provide appropriate functionality. Thus, applying coating on the implant surface is one of the most important technological techniques to provide the surface with chemical and physical properties that will contribute to the overall increase in the biocompatibility of the entire implanted product. Among the methods that are being actively researched and are becoming widespread in the application of biocompatible coatings from powders and wires, microplasma spraying (MPS) is distinguished [5, 6].

Zirconium-based alloys are increasingly being used as materials to improve the biocompatibility of implants due to their unique properties, such as the formation of an internal bone-like layer of apatite on their surface in the body, lower artefactuality in diagnistics by means of magnetic resonance imaging due to low magnetic susceptibility, as well as their excellent overall biocompatibility, high mechanical properties and corrosion resistance in body biological fluids [7, 8].

In addition to the chemical composition of the coating, the process of osseointegration is significantly influenced by the developed relief of its surface, the presence and size of open pores in the coating [9].

In [10], it is reported that a pore size of more than 100 μm is necessary for a successful bone formation process, while the recommended pore size should be about 300 μm. A similar pore size in the range of 200–400 μm is reported in [11] as a one promoting osteoblast adhesion, migration, and proliferation. The morphology of the surface microstructure also contributes to the conditions for cell adhesion on it. It was determined that microscale topography has a number

of advantages. For example, the micron size of the open pores can improve the roughness and surface area, as well as increase the contact between the implant and the bone. This effect of interaction between the implant and the bone, as was shown by the research results, largely contributes to osseointegration. In addition, the microlevel topography can block and stabilise fibrin flow, which can attract osteoprogenitor cells to colonise at the implant-bone interface. Most importantly, microscale surface topography can improve initial cell adhesion and differentiation [12].

Thus, V.E. Li confirms that micro- and nanoroughness of the contacting surface with the bone work synergistically to increase the efficiency of osseointegration of orthopaedic implants [13]. The results of histological studies show that a rougher surface relief promotes osseointegration processes [14].

K. Matsuzaka evaluated the effect of implant surface on the proliferation of osteoblast-like cells and showed that cells are fixed on surfaces depending on their relief, and their predominant number was observed on protrusions over 5 μm [15].

It is also indicated in [16] that with an increase in the surface roughness of the coating from R_a = 3.7 μm to 56.1 μm, the bonding of a titanium implant with a bone tissue increases by 4 times (from 5.38 ± 1.96 to 21.63 ± 2.51 MPa, respectively).

At present, the recommended average surface roughness for titanium orthopaedic implants is in a wide range (0.07–100 μm) [17], but systematic study of the effect of surface roughness on biocompatibility was not conducted. The authors of [17] indicated that the optimal range of surface roughness of orthopaedic implants should be 20–25 μm. Although an increase in the roughness index improved the adhesion and cell proliferation on the surface of Ti13Nb13Zr alloy samples in their experiment, it also increased the areas with stress concentration, worsening the bending strength and contributing to the formation of cracks. In [18], it is noted that the high roughness R_a = = 118.19 ± 9.06 μm of the surface of orthopaedic titanium implants can interfere with cell proliferation. It is assumed that a decrease in the rate of cell proliferation on base samples with increased roughness may be the result of an unfavourable biological reaction to increased interaction with titanium. Thus, the poor osseointegration of titanium implants may be caused by the effect of titanium on the surrounding tissues.

The literature presents different approaches to the selection of the optimal range of surface roughness of orthopaedic implants. Accordingly, using the recommended indices of roughness, in the future it will be necessary to investigate the produced surfaces for biocompatibility.

Table 1. Limit values of the studied parameters of the MPS process of Zr–Nb coating

Parameters	max (+)	min (–)
Current I, A	26	16
Plasma-forming gas flow rate Q_m, l/h	240	160
Spraying distance H, mm	120	40
Wire feed rate V_w, m/min	4.8	2.9

THE AIM

of this work is to investigate the elemental composition of the surface of the coating applied by microplasma spraying of Zr–Nb alloy wire onto the Ti6A14V alloy base, its topography, index of corrosion resistance in the environment similar to the human body, and adhesion strength to the base.

MATERIALS, EQUIPMENT, AND EXPERIMENTAL PROCEDURES

The formation of Zr–Nb alloy coatings from a wire with a diameter of 0.3 mm was carried out on a set of the MPS-004 equipment for microplasma spraying [19] on samples of Ti6A14V alloy.

Previously, as a result of the analysis of the calculated feed rate of Zr–Nb alloy wire, the required amount of heat of the microplasma jet, and practical experience in producing biocompatible coatings in the MPS-004 installation, the limit values of the MPS mode parameters were determined (Table 1) for further study of their influence on the process of forming biocompatible coatings from Zr–Nb alloy.

When determining the limit values of the MPS technological parameters, it was taken into account that at a current below 16 A and a plasma gas flow rate of less than 160 l/h, the thermal and gas-dynamic characteristics of the jet would not be sufficient to ensure the melting process of a 0.3 mm diameter Zr–Nb wire with its stable dispersion [19]. Therefore, the criteria for the limit values of the mode parameters were also selected taking into account the possibility of ensuring of both spraying as well as coating formation processes.

X-ray diffraction studies and chemical analysis were performed in the D8 ADVANCE Bruker diffractometer (Bruker, USA). The coatings were scanned at a voltage of 30 kV and at a magnification of ×200.

The surface morphology of the formed coatings was studied by analysing the obtained images in the Philips SEM515 using BE+SE sensors, an acceleration voltage of 20 kV and an electrode heating current of 40 mA.

Photos of the 3D profiles of the coating surfaces were obtained by means of the Huvitz HDS-2520 optical profiler (Gyeonggi, Republic of Korea) with a resolution of ± 0.1 μm at optical magnification of

Table 2. Chemical composition of Zr–Nb coating surface produced at MPS parameters I = 16 A; Q_m = 160 l/h; H = 40 mm; V_w = 2.9 m/min

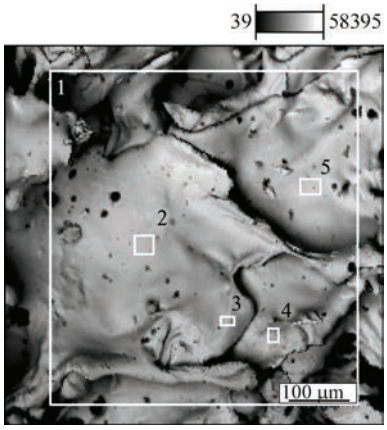

Scanning area	Content of chemical elements, at.%			
	Al	Ca	Zr	Nb
1	0.4	0.3	97.2 ± 0.9	2.1 ± 0.3
2	0.2	–	98.1 ± 0.8	1.7 ± 0.3
3	0.2	–	97.5 ± 0.8	2.3 ± 0.3
4	0.3	0.4 ± 0.1	97.5 ± 0.8	1.8 ± 0.3
5	0.2	–	97.7 ± 0.8	2.1 ± 0.3

×5, ×20, and ×50. The scanning area for each measurement was randomly selected to ensure reproducibility of the measurements and was approximately 700×500 µm². Area roughness parameters were chosen because they provide more informative values than line parameters.

The study of the 3D surface topography and the surface roughness parameter of the coatings over the area of 2D maps was carried out using Mountains® 9 software (Digital Surf, Besançon, France). The arithmetic mean deviation of the surface roughness profile (S_α) of the coatings was determined within a standard deviation of ± 0.1 µm in accordance with ISO 25178-2:2021.

The corrosion resistance of the coatings on 20×15×2 mm samples was studied for 1 h in a concentrated solution of 0.9 % NaCl with a concentration of ions close to human blood plasma. In the configuration of the electrical circuit, the samples under study acted as working electrodes, while the reference electrode was a platinum electrode. The Tafel extrapolation values were used to determine the corrosion current density (I_{corr}) and corrosion potential (E_{corr}). The polarisation curves were obtained in a solution of 0.9 % NaCl at 20 °C in the voltage range of –250–+250 mV and a scanning rate of 1 mV/s.

The adhesion strength of the coating to the base was determined using the static uniaxial tensile method in accordance with ASTM C633-13:2021. The number of tested coated samples was not less than 5 pcs. Tensile tests of each set of bonded sample assemblies were performed in a universal mechanical machine 2054 P-5 (SPC TechMash) at the same loading speed of 2 mm/min.

RESEARCH RESULTS AND DISCUSSION

The studies of the chemical composition of the surface of Zr–Nb coatings (Table 2) showed that they are similar to the initial material, which includes Zr, the average value of which is about 97.6 ± 0.82 at.% and Nb 2 ± 0.3 at.%, which corresponds to the industrial zirconium KTZ-125 alloy. Also, a small amount of Al and Ca was recorded, the content of which was less than 1 at.%, which can be considered as impurities in the composition of Zr–Nb alloy.

X-ray phase studies of Zr–Nb wire and surfaces of coated samples are presented in the form of X-ray diffraction patterns (Figure 1).

Comparing the X-ray diffraction patterns, it was found that complete melting of Zr–Nb wire in the microplasma jet and subsequent cooling of the dispersed particles on the surface of the base leads to the formation of coatings consisting of α-solid Zr solution with the presence of ZrO_2 oxide, ZrN nitride and $ZrNbC_2$ carbide inclusions.

The intensity of the peaks on the X-ray diffraction pattern and the similarity of the detected phases do not change with the variation of the MPS mode parameters and are observed on all coated samples. In terms of inclusion content in the coating, ZrO_2 phase prevails, which will further act as an inhibitor of the dissolution rate of the coating when it contacts with the surrounding fluids of the human body. The detected ZrN phase indicates the nitrogen saturation of

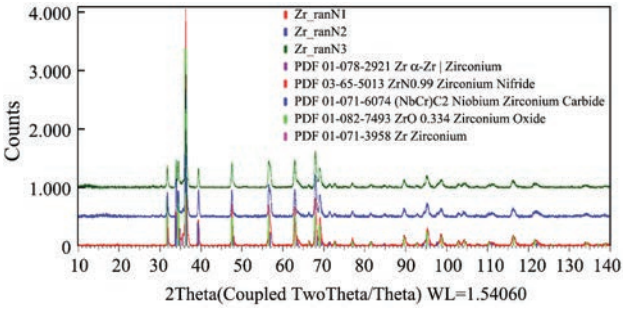

Figure 1. X-ray diffraction pattern of Zr–Nb coatings at MPS parameters: mode *1* — I = 26 A, Q_m = 240 l/h, H = 120 mm, V_w = = 4.8 m/min; mode 2 — I = 26 A, Q_m = 160 l/h, H = 40 mm, V_w = = 4.8 m/min; mode 3 — I = 16 A, Q_m = 160 l/h, H = 40 mm, V_w = = 2.9 m/min

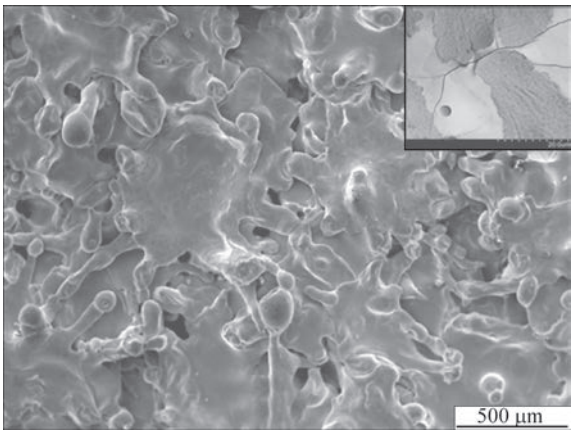

Figure 2. SEM morphology of Zr–Nb coating surface produced at MPS parameters I = 16 A; Q_m = 160 l/h; H = 40 mm; V_w = 2.9 m/min

the atomised particles when moving in the microplasma jet at a temperature of 670 K. This indicates that protection in the form of blowing a microplasma flux with atomised Zr particles by a stream of argon process gas is not sufficient to effectively separate them from atmospheric gases during coating formation. The presence of $ZrNbC_2$ inclusions in biocompatible coatings can contribute to an increase in the hardness of these coatings, but at the same time reduce their plasticity and adhesion strength to the base, as well as inclusions of oxides and nitrides.

It is known that both the size and pore content in the volume of the structure of Zr–Nb coatings as well as the microrelief of their surface layers are affected by the state and deformation of dispersed particles forming the coating, which in turn is determined by the parameters of the MPS mode [20]. The volume porosity content in the structure of Zr–Nb coatings was in the range of (2.8 ± 0.1) – (20.3 ± 2.0) %, while the highest volume porosity content in Zr–Nb coatings was formed on the mode with parameters I = 16 A; Q_m = 160 l/h; H = 40 mm; V_w = 2.9 m/min [20].

The study of the surface morphology of Zr–Nb coatings (Figure 2) showed that it is characterised by heterogeneity with many surface branches in the form of depressions and protrusions and open macropores

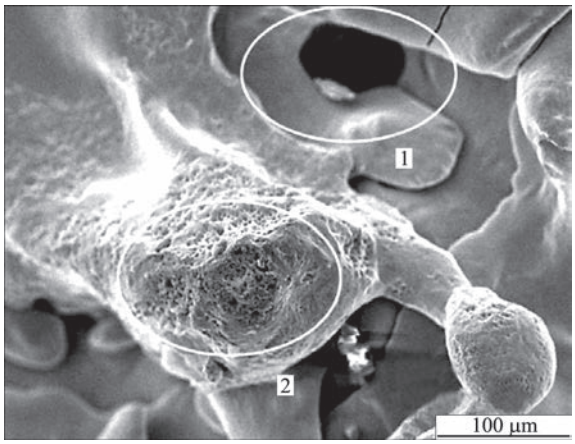

Figure 4. Morphology of the surface with macro- (*1*), micro- (*2*) pores of Zr–Nb coating formed at MPS parameters I = 16 A; Q_m = = 160 l/h; H = 40 mm; V_w = 2.9 m/min

of up to 300 ± 50 μm in size. Due to the dispersed particles, which were completely molten, Zr–Nb coatings were formed from disc-like splats. Due to the presence of residual stress in splats, the surface of Zr–Nb coatings had microcracks that formed due to rapid heat transfer and cooling processes. The formed cracks lead to the stress relaxation in the coating, while the porosity itself can be a way to reduce the modulus of elasticity of the coating and bring it closer to the bone, but it is also a dangerous factor that intensifies the degradation process at the interface between the coating and the base [21].

The surfaces of Zr–Nb coatings with the most pronounced microrelief had a roughness of S_α = 17 ± ± 0.1 μm (Figure 3).

A similar index of surface roughness, which promotes osseointegration processes, was obtained in [22] for a biocompatible titanium coating.

The study of the morphology of the surfaces of Zr–Nb coatings revealed not only open macropores up to 300 μm in size, but also micropores of up to 10 μm in size, which were located on the apexes of the coating protrusions formed from partially deformed dispersed particles from Zr–Nb wire (Figure 4).

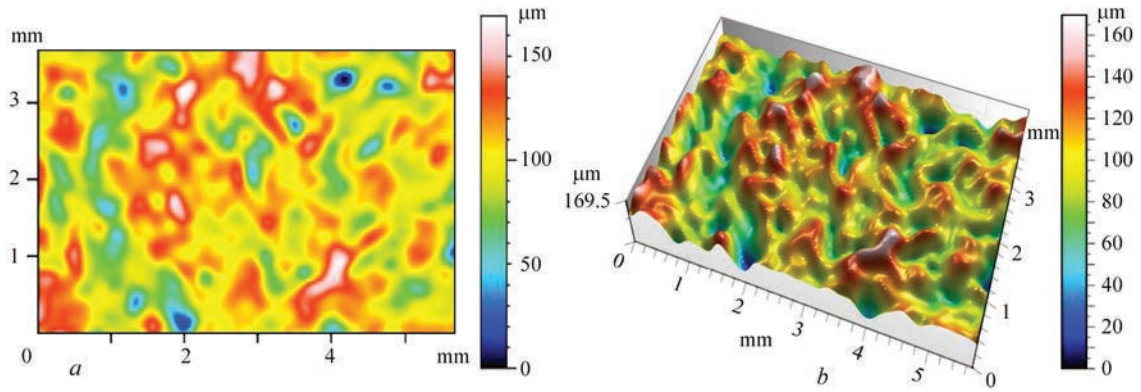

Figure 3. 2D (*a*) and 3D (*b*) topography of the surface microrelief of Zr–Nb coating produced at MPS parameters I = 16 A; Q_m = = 160 l/h; H = 40 mm; V_w = 2.9 m/min

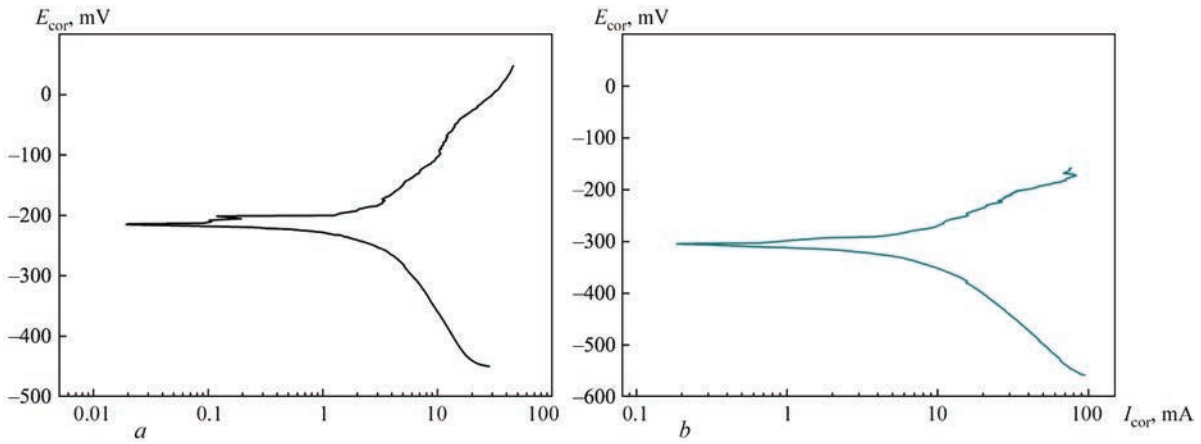

Figure 5. Polarisation diagrams of the dependence of the anode corrosion current density of Zr–Nb-coated samples (*a*) and Ti6A14V alloy base samples (*b*)

According to the literature, the results of the detected roughness and porosity will allow increasing the biocompatibility of the coating surface and ensuring a stronger bone-implant bonding due to the presence of places for fixation of the bone matrix and acceleration of the osseointegration process [23].

The carried out studies of the adhesion strength of Zr–Nb alloy coatings applied to the surface of Ti6A14V alloy samples showed that its average value for coatings with a thickness of 300 ± 10 μm with a volume pore content of 20.3 ± 2.0 % was 26 ± 2.1 MPa. Since there is currently no standard that defines the required adhesion strength of biocompatible Zr–Nb coatings with a porous structure to the surface of implants, their comparison was performed in accordance with the established requirement in the international quality standard ISO 13179-1:2021 for porous titanium coatings produced by plasma spraying on Ti6A14V alloy surfaces. According to the requirement of ISO 13179-1:2021, the average tear strength of a biocompatible coating should be more than 22 MPa. Therefore, the established adhesion of 26 ± 2.1 MPa, which characterises the adhesion strength of Zr–Nb coating to Ti6A14V alloy base, meets the requirements of ISO 13179-1:2021.

The results of studies of the corrosion resistance of Zr–Nb coating produced by the MPS method and from Ti6A14V alloy of the base after gas-abrasive treatment are presented in the form of polarisation diagrams (Figure 5).

From the analysis of polarisation curves, it was found that the plateau of the corrosion potential of Zr–Nb coating was about 216 mV and was in a more positive region of values than for Ti6A14V alloy base, which was 310 mV. Thus, the corrosion resistance of Zr–Nb-coated sample was higher than that of Ti6A14V alloy, which is explained by the presence of a protective surface oxide layer of ZrO_2, which reduces the corrosion rate by minimising the release of ions into the biological environment and promotes the process of osseointegration. Based on these characteristics, zirconium and its alloys were proposed as candidates for permanent implants [24].

An increased corrosion resistance mechanism is also facilitated by a film of niobium oxide (Nb_2O_5), which is formed along the boundaries of zirconium dioxide crystals and promotes "healing" of defects in the protective zirconium oxide film [25].

For all the studied samples of Zr–Nb coating and Ti6A14V alloy base, the anodic slope of the curve was similar to the cathodic slope of the curve in the polarisation diagram, which indicates that the kinetics of electron transfer for both the anodic and cathodic components is the same for both cases. The lower value of corrosion current density on Zr–Nb-coated samples (Figure 5, *a*) indicates a significantly lower rate of the corrosion process, which confirms the better efficiency of the surface layer protection by ZrO_2 oxide film. The similar results are given in [26] on the example of protecting the surfaces of magnesium alloys from corrosion in the human body, where ZrO_2 oxide film is recognised as more effective than TiO_2.

From the obtained results of the corrosion behaviour of the studied samples and their analysis, it was found that biocompatible Zr–Nb coatings produced by the MPS method will allow for much more effective corrosion resistance in biological solutions and an increase in the corrosion resistance of Ti6A14V alloy, which is currently most commonly used in the manufacture of implants.

CONCLUSIONS

1. It was determined that using the microplasma spraying method on the mode with parameters I = = 16 A, Q_m = 160 l/h, H = 40 mm, V_w = 2.9 m/min, the formation of Zr–Nb coating with the most developed microrelief with a roughness of S_a = 17 ± 0.1 μm is ensured. In addition, the presence of both macropores of up to 300 μm in size

and micropores of up to 10 μm in size was found on the surface of a porous Zr–Nb coating.

2. X-ray diffraction studies of Zr–Nb coatings showed that they consist of an α-solid solution of Zr with the presence of oxide (ZrO_2 — prevailing number), nitride (ZrN) and carbide (ZrN_BC_2) inclusions.

3. The obtained indices of corrosion resistance of Zr–Nb alloy coating samples in a solution of 0.9 % NaCl showed that the plateau of the coating corrosion potential was in a more positive region of values than for Ti6A14V alloy samples, which implies the formation of a passive layer that is a protective barrier against corrosion. The lower corrosion current density on Zr–Nb coating samples indicates their higher electrochemical resistance to corrosion and indicates a significantly lower rate of the corrosion process, which confirms the better efficiency of the surface layer protection by ZrO_2 oxide film.

4. As a result of the study of the adhesion strength of Zr–Nb coatings with a thickness of 300 ± 10 μm with a porous structure (pore content was 20.3 ± 2.0 % in the coating volume) with the surface of Ti6A14V alloy samples, an average adhesion strength of 26 ± 2.1 MPa was obtained, which meets the requirements of ISO 13179-1:2021 (over 22 MPa) and allows them to be used in accordance with the requirements of biocompatible titanium coatings on implant surfaces.

ACKNOWLEDGEMENT

The published results were obtained within the framework of the project No. 183/0070 dated 01.08.2024 “Development of innovative biocompatible antibacterial coatings and technology for their application to orthopaedic implants for using in the treatment of injuries in military personnel and civilians” with the grant support of the National Research Foundation of Ukraine within the framework of the competition “Science for Strengthening the Defence Capability of Ukraine”.

REFERENCES

1. Abd-Elaziem, W., Darwish, M.A., Hamada, A., Daoush, W.M. (2024) Titanium-based alloys and composites for orthopaedic implants applications: A comprehensive review. *Materials & Design,* **241**, 112850. DOI: https://doi.org/10.1016/j.matdes.2024.112850
2. Quinn, J., McFadden, R., Chan, C.-W., Carson, L. (2020) Titanium for orthopaedic applications: An overview of surface modification to improve biocompatibility and prevent bacterial biofilm formation. *Science*, 23(**11**), 101745. DOI: https://doi.org/10.1016/j.isci.2020.101745
3. Tepla, T., Pleshakov, E., Sieniawski, J., Bohun, L. (2022) Causes of degradation of titanium dental implants. *Ukrainian J. of Mechanical Engineering and Mater. Sci.*, 8(**4**), 31–40. DOI: https://doi.org/10.23939/ujmems2022.04.031
4. Wang, H., Liu, J., Wang, C. et al. (2020) The synergistic effect of 3D-printed microscale roughness surface and nanoscale feature on enhancing osteogenic differentiation and rapid osseointegration. *J. of Mater. Sci. & Technology*, **63**, 18–26. DOI: https://doi.org/10.1016/j.jmst.2019.12.030
5. Alontseva, D.L., Ghassemieh, E., Voinarovych, S. et al. (2019) Characterisation of the microplasma spraying of biocompatible coating of titanium. *J. of Microscopy*, 279(**3**), 148–157. DOI: https://doi.org/10.1111/jmi.12849
6. Woźniak, A., Staszuk, M., Reimann, Ł. et al. (2021) The influence of plasma-sprayed coatings on surface properties and corrosion resistance of 316L stainless steel for possible implant application. *Archives of Civil and Mechanical Engineering*, 21(**4**), 148. DOI: https://doi.org/10.1007/s43452-021-00297-1
7. Mehjabeen, A., Song, T., Xu, W. et al. (2018) Zirconium alloys for orthopaedic and dental applications. *Advanced Engineering Materials*, 20(**9**), 1800207. DOI: https://doi.org/10.1002/adem.201800207
8. Zhou, F.Y., Wang, B.L., Qiu, K.J. et al. (2012) Microstructure, mechanical property, corrosion behavior, andin vitrobiocompatibility of Zr–Mo alloys. *J. of Biomedical Materials Research Pt B: Applied Biomaterials*, 101B(**2**), 237–246. DOI: https://doi.org/10.1002/jbm.b.32833
9. Stich, T., Alagboso, F., Křenek, T. et al. (2021) Implant-bone-interface: Reviewing the impact of titanium surface modifications on osteogenic processes in vitro and in vivo. *Bioengineering & Translational Medicine*, **7**, e10239. DOI: https://doi.org/10.1002/btm2.10239
10. Cheikho, K., Laurent, C., Ganghoffer, J.F. (2022) An advanced method to design graded cylindrical scaffolds with versatile effective cross-sectional mechanical properties. *J. of the Mechanical Behavior of Biomedical Materials*, **125**, 104887. DOI: https://doi.org/10.1016/j.jmbbm.2021.104887
11. Wang, R., Ni, S., Ma, L., Li, M. (2022) Porous construction and surface modification of titanium-based materials for osteogenesis: A review. *Frontiers in Bioengineering and Biotechnology*, **10**, 973297. DOI: https://doi.org/10.3389/fbioe.2022.973297
12. Wang, H., Liu, J., Wang, C. et al. (2020) The synergistic effect of 3D-printed microscale roughness surface and nanoscale feature on enhancing osteogenic differentiation and rapid osseointegration. *J. of Mater. Sci. & Technol.*, **63**, 18–26. DOI: https://doi.org/10.1016/j.jmst.2019.12.030
13. Li, B.E., Li, Y., Min, Y. et al. (2015) Synergistic effects of hierarchical hybrid micro/nanostructures on the biological properties of titanium orthopaedic implants. *RSC Advances*, 5(**61**), 49552–49558. DOI: https://doi.org/10.1039/c5ra05821j
14. Cheng, B., Niu, Q., Cui, Y. et al. (2017) Effects of different hierarchical hybrid micro/nanostructure surfaces on implant osseointegration. *Clinical Implant Dentistry and Related Research*, 19(**3**), 539–548. DOI: https://doi.org/10.1111/cid.12471
15. Matsuzaka, K., Frank Walboomers, X., Yoshinari, M. et al. (2003) The attachment and growth behavior of osteoblast-like cells on microtextured surfaces. *Biomaterials*, 24(**16**), 2711–2719. DOI: https://doi.org/10.1016/s0142-9612(03)00085-1
16. Nakashima, Y., Hayashi, K., Inadome, T. et al. (1997) Hydroxyapatite-coating on titanium arc sprayed titanium implants. *J. of Biomedical Materials Research*, 35(**3**), 287–298. DOI: https://doi.org/10.1002/(sici)1097-4636(19970605)35:3%3C287::aid-jbm3%3E3.0.co;2-d
17. Jahani, B. (2021) The effects of surface roughness on the functionality of Ti13Nb13Zr orthopedic implants. *Biomedical J. of Scientific & Technical Research*, 38(**1**), 30058–30067. DOI: https://doi.org/10.26717/bjstr.2021.38.006104
18. Lewallen, E.A., Trousdale, W.H., Thaler, R. et al. (2021) Surface roughness of titanium orthopaedic implants alters the

biological phenotype of human mesenchymal stromal cells. *Tissue Engineering Pt A*, **27**, 1503–1516. DOI: https://doi.org/10.1089/ten.tea.2020.0369
19. Borisov, Yu.S., Kislitsa, A.N., Vojnarovich, S.G. (2006) Peculiarities of the process of microplasma wire spraying. *The Paton Welding J.*, **4**, 21–25.
20. Voinarovych, S.G., Alontseva, D.L., Kyslytsia, O.N. et al. (2021) Fabrication and characterization of Zr microplasma sprayed coatings for medical applications. *Advances in Mater. Sci.*, 21(**2**), 93–105. DOI: https://doi.org/10.2478/adms-2021-0013
21. Fousova, M., Vojtech, D., Jablonska, E. et al. (2017) Novel approach in the use of plasma spray: Preparation of bulk titanium for bone augmentations. *Materials*, 10(**9**), 987. DOI: https://doi.org/10.3390/ma10090987
22. Alontseva, D., Ghassemieh, E., Voinarovych, S. et al. (2020) Manufacturing and characterisation of robot assisted microplasma multilayer coating of titanium implants: Biocompatible coatings for medical implants with improved density and crystallinity. *Johnson Matthey Technology Review*, 64(**2**), 180–191. DOI: https://doi.org/10.1595/205651320x15737283268284
23. Cheikho, K., Laurent, C., Ganghoffer, J.F. (2022) An advanced method to design graded cylindrical scaffolds with versatile effective cross-sectional mechanical properties. *J. of the Mechanical Behavior of Biomedical Materials*, **125**, 104887. DOI: https://doi.org/10.1016/j.jmbbm.2021.104887
24. Rosalbino, F., Macciò, D., Scavino, G. (2023) Corrosion behaviour of Zr–Ag alloys for dental implant application. *Mater. Sci. and Applications*, 14(**11**), 501–514. DOI: https://doi.org/10.4236/msa.2023.1411033
25. Kirichenko, V.G. (2015) *Nuclear physics of metal sciences of power engineering alloys.* Chapt. 1, Kharkiv, KhNU [in Russian].
26. Peron, M., Bertolini, R., Cogo, S. (2022) On the corrosion, stress corrosion and cytocompatibility performances of ALD TiO_2 and ZrO_2 coated magnesium alloys. *J. of the Mechanical Behavior of Biomedical Materials*, **125**, 104945. DOI: https://doi.org/10.1016/j.jmbbm.2021.104945

ORCID
S.Yu. Maksymov: 0000-0002-5788-0753,
S.G. Voinarovych: 0000-0002-4329-9255,
S.N. Kaliuzhnyi: 0000-0002-8132-3930,
O.N. Kyslytsia: 0000-0001-8894-4660,
I.S. Sviridova: 0009-0005-6302-3423,
L. Alontseva: 0000-0003-1472-0685,
Ridvan Yamanoglu: 0000-0002-4661-8215

CONFLICT OF INTEREST
The Authors declare no conflict of interest

CORRESPONDING AUTHOR
S.Yu. Maksymov
E.O. Paton Electric Welding Institute of the NASU
11 Kazymyr Malevych Str., 03150, Kyiv, Ukraine.
E-mail: serge.voy@gmail.com

SUGGESTED CITATION
S.Yu. Maksymov, S.G. Voinarovych, S.N. Kaliuzhnyi, O.N. Kyslytsia, I.S. Sviridova, L. Alontseva, R.Yamanoglu (2024) Coating for medical application produced by microplasma spraying from Zr–Nb alloy. *The Paton Welding J.*, **12**, 3–9.
DOI: https://doi.org/10.37434/tpwj2024.12.01

JOURNAL HOME PAGE
https://patonpublishinghouse.com/eng/journals/tpwj

Received: 09.09.2024
Received in revised form: 29.10.2024
Accepted: 26.12.2024